# Revealing and optimizing the design of covers for outdoor units of air-conditioners in highrise residential buildings through CFD simulations, thermodynamic modeling and performance measurements

Jiyuan Wu[1], Lan Wang[1], Tianzhen Hong[2], Wei Wang[1]
[1]School of Architecture, Southeast University, Nanjing, Jiangsu Province, China 210096, [2]Building Technology and Urban Systems Division, Lawrence Berkeley National Laboratory, 1 Cyclotron Road, Berkeley, CA, 94720, USA

Disclaimer:

# Revealing and optimizing the design of cover installation for outdoor units of air conditioners through CFD simulations and thermodynamic modeling

Jiyuan Wu [a], Lan Wang [a], Tianzhen Hong [b], Qinran Hu [c], Wei Wang [a,d,*]

[a] *School of Architecture, Southeast University, Nanjing, Jiangsu Province, 210096, China*
[b] *Building Technology and Urban Systems Division, Lawrence Berkeley National Laboratory, 1 Cyclotron Road, Berkeley, CA, 94720, USA*
[c] *School of Electrical Engineering, Southeast University, Nanjing, Jiangsu Province, 210096, China*
[d] *Key Laboratory of Urban and Architectural Heritage Conservation (Southeast University), Ministry of Education, China*

ARTICLE INFO

ABSTRACT

When renewing building facades in most Chinese cities, covers are often designed and installed to conceal the outdoor units of residential split air conditioners for congruousness of building facades. However, how those covers impact airflow and energy efficiency should be thoroughly examined. This study investigates two popular designs of cover (louver and circular-hole) and selects Nanjing, renowned for its hot summers, as the case city. This study employs Computational Fluid Dynamics models to simulate airflow obstruction caused by the covers surrounding the outdoor units. Grey Model, trained from the CFD results, quantifies interactions between design of cover and inlet air temperature. Additionally, a thermodynamic model assesses the covers' impact on the coefficient of performance of air conditioners. The findings reveal that the primary cause of outdoor unit overheating is warm air backflow from the outlet to the inlet. A mere 1 °C increase in inlet air temperature can reduce COP by 4.1%–8.7%. The maximum temperature differences caused by different designs of cover are 4.5 °C for the louver type and 4.4 °C for the circular-hole type. To mitigate these negative impacts, optimal design recommendations are provided: a minimum distance between the cover and outdoor unit of 0.29 m for louver type and 0.1 m for circular-hole type, both feasible in most installations. These findings can help designers, manufacturers, installers and policymakers, to facilitate the design and installation of optimal covers for outdoor air-conditioning units, thus minimizing energy efficiency losses.

## Nomenclature

*Roman symbols*

| | |
|---|---|
| $h_m$ | The coefficient of convection heat transfer (W/(m²·K)) |
| $h$ | Enthalpy (kJ/kg) |
| $l$ | Characteristic length (m) |
| $Pr_m$ | Prandtl Number |

| $Re_m$ | Reynolds Number |
|---|---|
| *Greek symbols* | |
| $\varphi$ | Heat flux (kW) |
| $\lambda_m$ | Thermal conductivity (W/(m·K)) |
| | |
| *Indices* | |
| condenser | Heat exchange on condenser |
| compressor | Heat exchange on compressor |
| evaporator | Heat exchange on evaporator |
| inside | The coefficient of convection heat transfer on the inside of the pipe |
| outside | The coefficient of convection heat transfer on the outside of the pipe |
| throttle | Heat exchange on throttle |
| | |
| *Acronyms* | |
| AC | Air Conditioning |
| CFD | Computational Fluid Dynamics |
| COP | Coefficient of Performance |
| GA | Genetic Algorithm |
| GM (1,1) | Grey Model of first-order equation with one variable |
| HVAC | Heating, Ventilation and Air Conditioning |

## 1. Introduction

Over the past eight years, global temperatures have consistently soared and in 2022, the global average temperature is about 1.15 °C above pre-industrial levels marking years from 2015 to 2022 as the hottest five years on record [1]. Climate change has precipitated a recurring surpassing of urban temperature records worldwide. Consequently, air conditioner (AC) has become a necessity for thermal survivability of residents. Statistics reveal a significant increase in the prevalence of AC per 100 urban households in China, reaching 161.7 units in 2021 with 41% increase from 2015's 114.6 units [2]. This surge parallels a substantial increase in the electricity consumption of split AC systems, escalating from 8.2 billion kWh in 2001 to surpassing 100 billion kWh in 2019 within urban areas [3]. Moreover, forecasts indicate an imminent global increase in electricity demand for space cooling in buildings, projected to potentially surge by 40% by 2030 [4]. Thus, the conservation of energy within AC systems stands as a pivotal component in building energy management.

The existing array of technologies and policy strategies aimed at enhancing the cooling efficiency of air conditioning systems is quite extensive. These approaches encompass solutions related to equipment, such as establishing minimum energy performance standards to regulate AC products [5,6], enhancing AC refrigeration and control technology [7,8], reducing cooling demand [9,10], and so on. Among these strategies, methods to enhance the efficiency of the refrigeration cycle have gained significant traction. The majority of AC systems used globally rely on vapor compression refrigeration cycle technology. To drive this cycle, the split AC used in buildings comprises four primary components: i) the evaporator, which is situated indoors and functions to remove heat from the indoor environment during summer and transfer heat indoors during winter; ii) the condenser, iii) the compressor, and iv) the valve, which are located in the outdoor unit. The condenser in the outdoor unit serve for releasing heat to the outdoor during summer and absorbing heat from the outdoor during winter [11]. Compressor and throttle valve in the outdoor unit mainly serve for the change in pressure of refrigerating fluid.

Therefore, efforts aimed at reducing the energy consumption of AC systems typically concentrate on the four primary components and the refrigeration system. For instance, Garayo et al. (2022) proposed an Heating, Ventilation and Air Conditioning (HVAC) system based on a thermoelectric air-to-air pump combined with a heat recovery unit, which could improve the COP of the heat pump: 2-3 times for partial load operation and 12.5% for maximum load [12]. Ghodbane et al. (2022) incorporated the hot storage tank into a solar AC between the evaporator and the condenser, which could reach 67.06% of thermal efficiency of solar collector and have a low electricity consumption [13]. Nagappan (2022) proposed an ejector in place of compressor in refrigeration system, which could consume less power about 2.475 kW than the traditional refrigeration system [14]. These technological advancements significantly enhance the cooling efficiency of AC systems by improving the refrigeration cycle. Another critical aspect within this cycle is the manner in which the AC refrigeration system exchanges heat between the indoor and outdoor environments, considering the substantial impact of the outdoor environment on indoor conditions.

When releasing the heat from building indoor to outdoor environment, the outdoor unit, a pivotal component of the AC system cycle of AC, assumes a crucial role. Particularly in hot summers, the substantial heat discharged through the outdoor unit of the AC system can significantly impact the urban thermal environment, exacerbating the urban heat island (UHI) effect and consequently reducing the efficiency of the refrigeration cycle [15–17]. Liang et al. (2018) proposed a zonal model to assess the airflow and air temperature within high-density urban street canyons, which shows that air temperature in the mock-up street canyons could increase up to 6 °C, suggesting that the thermal environment around the outdoor unit could be more awful [18]. Lee et al. (2014) summarized the causes of the UHI, confirming that large amounts of heat released through outdoor units of AC systems can lead to the formation of

ozone and smog, and make urban temperatures 5–12 °C warmer than surrounding countryside under extreme meteorological conditions [19]. Vahmani et al. (2022) distinguished between two major components of anthropogenic heating from HVAC and relief/exhaust air from buildings, which shows that when the daily maximum air temperature increases from 25 °C to 40 °C, the heat released through outdoor units could reach a peak of more than 500 W/m$^2$ of the land surface area [20]. A negative influence usually happen that the heat released through outdoor units will make the ambient temperature rise, the rising temperature also in turn increases the energy consumption of the AC system [21].

To mitigate negative influences, ensuring the proper installation of outdoor units is crucial. This involves designing a suitable shell, clearing their surroundings, and positioning them on rooftops and so on, to minimize heat accumulation. Upon this and other consideration like the outdoor units are incongruous with urban building facades, Chinese policymakers designed the cover to conceal outdoor units of residential split AC. Fig. 1 presented the typical cover in some Chinese cities. In these photos, the areas framed by the red lines are the cover around the outdoor units, which demonstrates this phenomenon is large-scale and organized. Unfortunately, proper installation is often overlooked. The obstruction of heat emission from outdoor units, such as when they're positioned within building gaps leading to heat accumulation, significantly impacts energy consumption [22]. Hsieh et al. (2011) discovered that mismanaging heat rejection from residential ACs exacerbates the urban thermal environment of canopy, subsequently increasing building energy usage [23]. In response, Chen et al. (2021) developed a wind-powered generator utilizing exhaust from outdoor units. This system prevents air backflow by directing the heat airflow upward [24]. Abdullah et al. (2022) explored the thermal plume effects of VRF outdoor units concealed in aluminum louvers. Removing these louvers proved an effective method to diminish thermal plume influence, reducing average suction temperatures by 8%–19% for VRF outdoor units across floors 10th to 12th [25]. Additionally, covers on the facades of buildings must increase the cost of building design and this increased cost in the design phase, which is not oriented towards energy conservation, will lead to increased costs in the operational phase [26]. Current research has proved the great negative impact of improper cover around the outdoor units on the operation of AC but seldom refer to the design of cover to reduce the impact. However, as a large-scale and organized phenomenon, it is impossible to dismantle all cover because of the cause of lot of material waste. Thus, if the cover has to be installed, how to design the proper cover is so much significant and lacks the reference from scientific research. This study aims to reveal the impact of cover on COP of AC and propose the suggestion for proper installation.

To comprehend the effect of these cover on AC systems, on-site measurements, and CFD serve as essential approaches. CFD, in particular, has found extensive application in simulating airflow, encompassing both indoor terminal and outdoor unit dynamics within AC systems [27]. Hou et al. (2022) devised a novel optimization method for organizing airflow, centered on identifying the suitable air supply angle. Their CFD simulations of nine different angles determined that the optimal air supply angle hovers around 35° [28]. Liu et al. (2021) explored enhancing the air-side heat transfer performance of outdoor AC units. Through CFD simulations across various working conditions, they achieved a notable 23.4% improvement in the heat transfer coefficient [29]. Hadavi et al. (2021) used three different density city models as case studies to study the simultaneous effect of urban morphology and density on outdoor-installed cooling system performance, and finally, concluded that decreasing urban compactness mitigates UHI intensity by allowing thermal wake sevacuation, which eventually provides up to 16.4% energy saving [30]. Yan et al. (2020) investigated the common installation methods of outdoor units in Chongqing, China, and discovered it could reduce the inlet air temperature for an average of 9.06 °C by setting up a partition board to separate the supply and exhaust air at the exhaust outlet of the outdoor unit [31].



**Fig. 1.** Photos of the typical covers on the outdoor units of AC in some Chinese cities.

However, CFD simulation typically demands substantial time investment. Moreover, the above research focuses on optimization via CFD simulation for specific scenarios, which can not encompass the ergodic searching of the structure optimization of the covers in this study. Hence, a method that expedites simulations or provides a wider array of solutions is crucial for optimizing cover structures.

To address the widespread practice of installing covers around outdoor AC units, this study aims to investigate the extent and manner in which these covers impact the energy performance of AC systems. Additionally, the study seeks to explore design strategies that can effectively minimize negative effects. First, after on-site investigation in Nanjing city, this study concludes two main cover types: louver and circular hole, and defines the structural factors for optimization, including distance between cover and outdoor unit for both types, louver angle and louver space for louver type, and percentage of exposure for circular-hole type, respectively. Second, this study establishes a CFD model using COMSOL software to analyze the relationship between the inlet air temperature of outdoor unit and various structural factors of cover. To streamline the CFD simulations and reduce time consumption, the Grey Model (GM (1,1)) is employed to predict outcomes for different design conditions, which is driven by the CFD simulation results of the inlet air temperature. Concurrently, thermodynamic cycle calculations for the AC system are utilized to indirectly gauge the impact of energy consumption attributed to covers around the outdoor units. Based on these analyses, the study aims to propose optimal structural design factors for these covers.

## 2. Material and methods

In this section, the methodology will be introduced in detail from the setup of CFD model to the calibration of simulation and ultimately to the prediction method. Final results in next section were obtained upon this methodology. For clarity, this section will be started by the overall introduction of the methodology.

### 2.1. Flowchart of this study

This study utilized the GM (1,1), driven by CFD simulation data, to derive the optimal design for the cover. Additionally, it
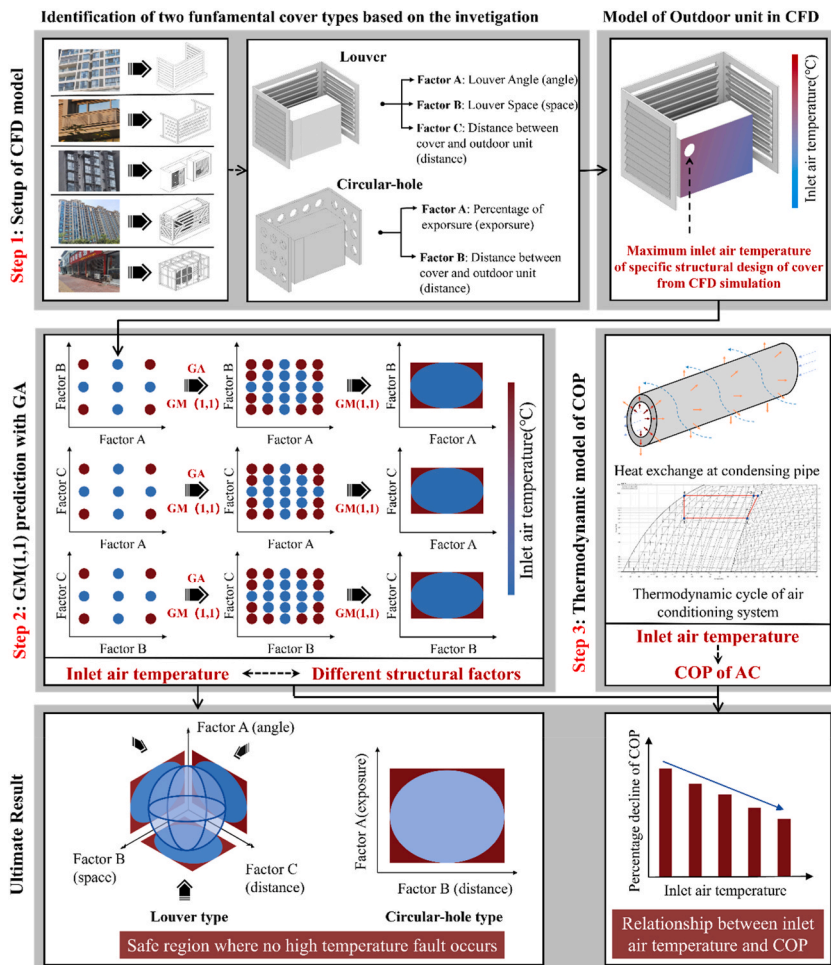


**Fig. 2.** Flow chart of GM (1,1) based on simulation data and thermodynamic model of AC.

established the thermodynamic cycle of the AC system to assess the cover impact on the Coefficient of Performance (COP). Fig. 2 shows the overall workflow of this study, encompassing three major steps.

● Step 1 (Setup of CFD model and calibration): Two fundamental cover types (louver type and circular-hole type) were identified based on investigation in Nanjing city. This study chose a typical outdoor unit with louver cover in Nanjing to establish the CFD model in COMSOL software for simulating the air flow and temperature distribution around the outdoor unit. Meanwhile, this study measured the inlet air temperature of this outdoor unit under normal operation in the ambient temperature of 34 °C. Through adjusting the physical parameters in the CFD model to make the relative error of the central inlet air temperature less than 5%. Additionally, this study determined the structural design of two cover types for the optimization process.

● Step 2 ((GM (1,1)) prediction with Genetic Algorithm): Subsequently, following the initial CFD simulations, the GM (1,1) was employed to extrapolate finite and discrete simulation data, predicting inlet air temperature data distributed across various structural design conditions. GM (1,1) have been proved to be effective in solving prediction problems for small amounts of data [32,33]. Although the relative error in this study has been less than 5%, the maximum absolute error of the prediction results is still over 1 °C. Thus, Genetic Algorithm (GA) was used to refine the GM (1,1), culminating in a representation of the relationship between inlet air temperature and structural factors. The method of combining GM (1,1) with other algorithms to meet different specific prediction needs has become a common method in research [34,35]. And GA has been proved to be effective to optimize the prediction model [36,37]. Therefore, GM (1,1) combined with GA could effectively meet the demand of this study for the accuracy of prediction results. Through this step, this study confirmed the safe regions of structural factors where the inlet air temperature is under the threshold temperature.

● Step 3 (Thermodynamic model of COP): This study established the stationary energy calculation for the thermodynamic cycle of a split AC system. In order to complete the energy calculation, the following simplification and assumptions are made in this study: first, in the refrigeration cycle, the enthalpy before and after the refrigerant flowing through the throttle valve is equal; second, compressor power does not change with the change of working environment temperature; third, the heat of refrigerating fluid in the condensing tube is completely transferred to the outside air and does not accumulate in the tube wall. Through the above
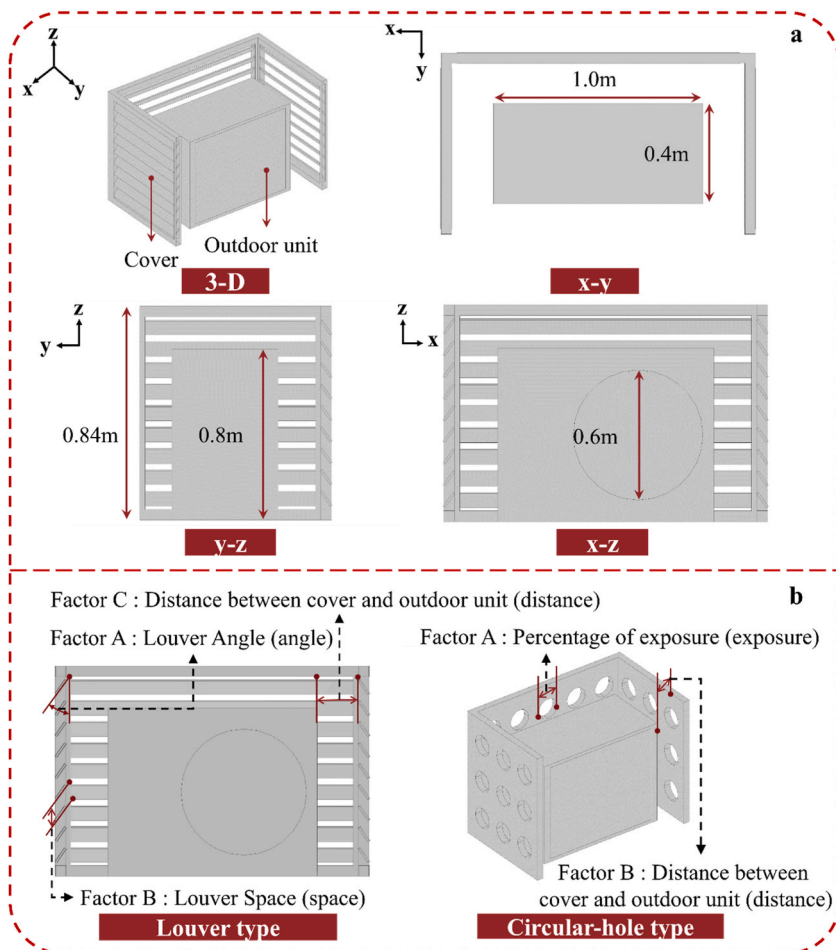


**Fig. 3.** Size of outdoor unit and structural factors of cover.

simplification and assumptions, the study integrated the heat release from the condensing tube of outdoor unit to the cooling capacity of AC systems. This evaluation aimed to determine the impact of varying outdoor unit inlet air temperatures on COP, thereby assessing the effect of different cover structural designs on COP. Through this step, this study obtained the relationship between inlet air temperature and COP and evaluated the influence of cover on the COP based on the results of step 2.

### 2.2. Illustration of simulation model

This study chose a standard outdoor unit commonly used in popular Chinese residential AC products as the case study. Fig. 3 presents the size of outdoor unit and structural factors of cover the sizes of both the outdoor unit and its cover are presented in Fig. 3(a). The CFD model primarily comprises the external environment, the outdoor unit, and the cover. The outdoor unit measures 0.32 m$^3$, featuring a circular-hole air outlet with a radius of 0.6 m. The external environment volume of simulation model is five times that of the outdoor unit. The vertical dimension of the cover is 0.84 m. Within the cover model, this study identified structural design factors for both the louver cover and the circular-hole cover, as depicted in Fig. 3(b). Regarding the louver cover, three factors were considered: the louver angle, louver space, and the distance between cover and outdoor unit. The ranges for three factors of the louver type were set at 5–85°, 0.05 m–0.40 m, and 0.15 m–0.40 m, respectively. Meanwhile, the circular-hole cover featured two structural design factors: the percentage of exposure (referring to the proportion of the total cover area occupied by the circular holes) and the distance between cover and outdoor unit. The variation ranges for the two factors of the circular-hole cover were 10%–50% and 0.15 m–0.40 m, respectively.

### 2.3. Configuration and calibration of simulation model

In this study, a non-isothermal flow model was employed to simulate the airflow around the covered outdoor unit of the AC system. This non-isothermal flow model incorporates the laminar flow regime and considers convective heat transfer based on wind speed and the characteristic length scale of the outdoor units. Quantifying the heat transfer between the air and the outdoor unit relies significantly on the convective heat transfer coefficient, $h_m$. This coefficient is influenced by variables such as the temperature difference between air and outdoor unit, and the air velocity. Following on-site measurements of an outdoor unit in Nanjing, where the cover is in the form of louver, the air velocity at the air outlet of outdoor unit measured 3 m/s. Concurrently, during stable operation of the AC system, the outlet air temperature was recorded at 51.5 °C, while the temperature of the outdoor unit casing stood at 49 °C. The external environment temperature was set at 34 °C, reflecting the average summer temperature in Nanjing as of August 2022. Based on these parameters, the convective heat transfer coefficient, $h_m$ was derived using Eq. (1):

$$h_m = \frac{\lambda_m \times 0.664 \times Re_m^{1/2} \times Pr_m^{1/3}}{l} \tag{1}$$

where $\lambda_m$ is thermal conductivity of air (W/(m·K)), $Re_m$ is Reynolds Number, $Pr_m$ is Prandtl Number, $l$ is characteristic length (m).

Fig. 4 displays the calibration results. This study modified the heat transfer dynamics between air and the outdoor unit to adjust the inlet air temperature, thereby refining the CFD simulation model. This adjustment involved fine-tuning the calculation parameters of the convective heat transfer coefficient. Post-calibration, the central inlet air temperature of the CFD model measured 43.6 °C, whereas the on-site measurement recorded 43.1 °C, resulting in a relative error of 1.16%. Consequently, the calibrated convective heat transfer coefficient stands at 12 W/(m$^2$•K), utilized in subsequent CFD simulations for various structural designs of the outdoor unit.

### 2.4. Thermodynamics of air conditioner system

The cover surrounding the outdoor unit notably impedes the outward flow of air from the outdoor unit into the external environment. This obstruction is particularly impactful during summer when the temperature of the air discharged from the outdoor unit is
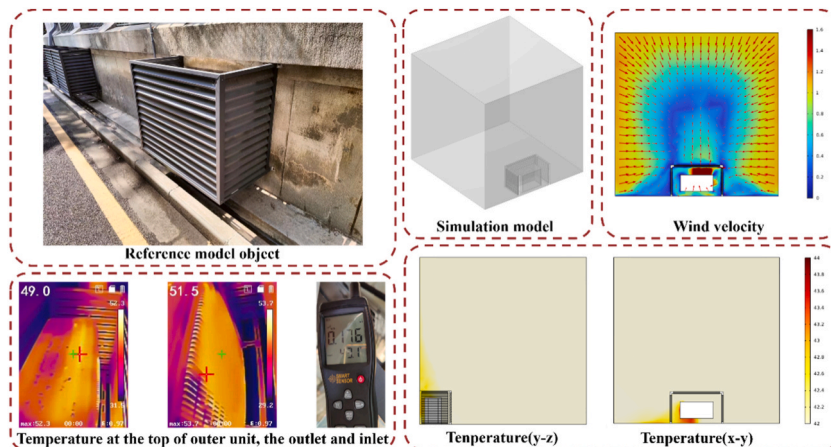


**Fig. 4.** Calibration results and object of a typical outdoor unit.

considerably higher than the external surroundings. Consequently, influenced by the cover, the accumulation of high-temperature air around the outdoor unit of the AC system adversely affects the working environment and compromises its performance. To address this, this study established an energy calculation for the thermodynamic cycle of the AC system and developed a mathematical relationship between the outdoor unit inlet air temperature and the system performance. This investigation utilized an air-cooled condenser employing R32 as the refrigerant. It is worth noting that if the inlet air temperature of the outdoor unit exceeds a certain protection threshold, the AC system will shut down.

### 2.4.1. Safe temperature determination

The condensing temperature is a crucial parameter in the refrigeration cycle as it directly affects the refrigeration effect, system safety, and energy consumption. When the inlet air temperature exceeds the condensing temperature, the latter must rise to maintain the system proper function. Consequently, the condensing pressure also increases to align with the higher condensing temperature, leading to an increased compression ratio of the refrigeration compressor making two primary effects. First, this elevation in pressure augments the power consumption of the compressor, subsequently reducing the COP of the AC system. Second, it raises the exhaust temperature of the compressor, thereby increasing the likelihood of system shutdown.

During the design of the AC system, the designer sets the condensing temperature ($t_k$) in the early stages of the process. This temperature is determined by the summer outdoor dry-bulb temperature and the temperature difference between the condensing temperature and the inlet air dry-bulb temperature in Eq. (2):

$$t_k = t_1 + \Delta t \tag{2}$$

where $t_1$ is the summer outdoor dry-bulb temperature (°C), $\Delta t$ is the temperature difference between the condensing temperature and the inlet air dry-bulb temperature (°C)

The $\Delta t$ ranges from 10 °C to 15 °C. The ambient temperature used in the CFD model for this study is based on the mean temperature recorded in Nanjing City in August 2022, which was 34 °C. Following the air conditioner system design regulations stipulated by the Chinese government [38], a safety threshold of 44 °C is established in this study. Consequently, if the inlet air temperature surpasses 44 °C, the AC system is compelled to raise the condensing temperature, consequently increasing the compression ratio of compressor, leading to a risk of triggering a high-temperature fault.

### 2.4.2. Numerical model between inlet temperature and COP

In the thermal cycle of the AC system, evaporation primarily occurs within the evaporator of indoor unit. Meanwhile, the compression, condensation, and throttling processes take place within the compressor, condenser, and throttling valve, respectively, situated in the outdoor unit. Following the principle of energy conservation, the thermodynamic cycle was concluded in Eq. (3):

$$h_{compressor} + h_{condenser} = h_{throttle} + h_{evaporator} \tag{3}$$

where $h_{compressor}$ is the enthalpy of heat exchange on compressor (kJ/kg), $h_{condenser}$ is the enthalpy of heat exchange on condenser (kJ/kg), $h_{throttle}$ is the enthalpy of heat exchange on throttle (kJ/kg), $h_{evaporator}$ is the enthalpy of heat exchange on evaporator (kJ/kg).

In an ideal scenario, the enthalpy prior to the throttling process was assumed to be equal to after. Thus, Eq. (3) was converted to Eq. (4):

$$h_{compressor} + h_{condenser} = h_{evaporator} \tag{4}$$

It was assumed that there is no refrigerant loss throughout circulation, which means the mass flow rate of refrigerant is constant and
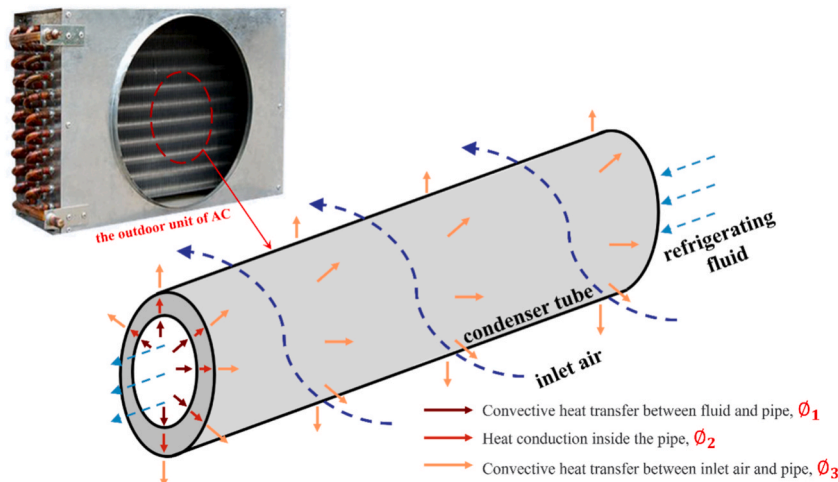


**Fig. 5.** Heat exchange from the refrigerating fluid to the air through the condenser tube.

Eq. (4) was converted to Eq. (5):

$$\varnothing_{evaporator} + \varnothing_{compressor} = \varnothing_{condenser} \tag{5}$$

where $\varnothing_{evaporator}$ is the heat flux of heat exchange on evaporator (kW), $\varnothing_{compressor}$ is the heat flux of heat exchange on compressor (kW), $\varnothing_{condenser}$ is the heat flux of heat exchange on condenser (kW).

When the inlet air temperature changes, both the $\varnothing_{evaporator}$ and $\varnothing_{condenser}$ undergo changes. Considering the increase in compressor energy consumption, $\varnothing_{evaporator}$ was expressed in terms of $\varnothing_{condenser}$. Ultimately, this allowed for the calculation of the relationship between $\varnothing_{condenser}$ and the inlet air temperature, providing the final relationship between $\varnothing_{evaporator}$ and the inlet air temperature, which further elucidates the relationship between the COP of the AC system and the outdoor unit inlet air temperature. Fig. 5 presents the heat exchange of condensation pipe. In summer, the refrigerating fluid transfer the heat to the condenser tube and the heat is ultimately absorbed by the air when the air flows around the tube, both of which is in the form of convective heat transfer.

$\varnothing_1$ represents the convective heat transfer between the refrigerant and the condenser tube for a condenser tube of unit length, denoted as $\varnothing_{condenser}$. $\varnothing_2$ denotes the heat conduction occurring within the tube, while $\varnothing_3$ signifies the convective heat transfer between the tube and the inlet air. Assuming the heat transfer process disregards the heat capacity of condensing tube and the anisotropy of each component, the temperatures of both the inner and outer wall surfaces of the pipe remain constant. Heat conduction occurs along the tube diameter. Following the principle of energy conservation, the convective heat transfer, $\varnothing_1$ between the refrigerant and the condenser tube equates to the heat conduction within the tube, $\varnothing_2$ in Eq. (6):

$$\varnothing_1 = \varnothing_2 \tag{6}$$

According to the convective heat transfer equation and the circular tube thermal conductivity, Eq. (6) was converted to Eq. (7):

$$2\pi r_1 \bullet dl \bullet h_{m,inside,j} \bullet (t_{fluid,j} - t_{W1}) = \frac{(t_{W1} - t_{W2})}{\frac{1}{2\pi\lambda \bullet dl} \bullet \ln\frac{r_2}{r_1}} \tag{7}$$

where $h_{m,inside,j}$ is the coefficient of convection heat transfer on the inside of the pipe at position j (W/(m$^2$·K)), $t_{fluid,j}$ is the temperature of refrigerating fluid at position j (°C), $t_{W1}$ is the temperature of pipe inner wall (°C), $t_{W2}$ is the temperature of pipe outer wall (°C), $\lambda$ is the thermal conductivity (W/(m·K)), $r_1$ is the pipe inner radius (m), $r_2$ is the pipe outer radius (m).

Eq. (7) can be simplified to Eq. (8):

$$r_1 \bullet h_{m,inside,j} \bullet (t_{fluid,j} - t_{W1}) = \lambda \bullet \frac{t_{W1} - t_{W2}}{\ln r_2 - \ln r_1} \tag{8}$$

The relationship between the heat conduction within the tube, $\varnothing_2$ and the convective heat transfer between the tube and the inlet air, $\varnothing_3$ was obtained by ignoring the effect of the heat capacity of the circular tube in the assumptions in Eq. (9):

$$\varnothing_2 = \varnothing_3 \tag{9}$$

According to the convective heat transfer equation and the circular tube thermal conductivity, Eq. (9) was converted to Eq. (10):

$$\frac{(t_{W1} - t_{W2})}{\frac{1}{2\pi\lambda \bullet dl} \bullet \ln\frac{r_2}{r_1}} = 2\pi r_2 \bullet dl \bullet h_{m,outside} \bullet (t_{air} - t_{W2}) \tag{10}$$

where $h_{m,outside}$ is the coefficient of convection heat transfer on the outside of the pipe (W/(m$^2$·K)), $t_{air}$ is the temperature of air (°C).

Eq. (12) can be simplified to Eq. (11):

$$r_2 \bullet h_{m,outside} \bullet (t_{air} - t_{W2}) = \lambda \bullet \frac{t_{W1} - t_{W2}}{\ln r_2 - \ln r_1} \tag{11}$$

Eq. (12) was obtained from Eq. (8) and Eq. (11):

$$r_2 \bullet h_{m,outside} \bullet (t_{air} - t_{W2}) = r_1 \bullet h_{m,inside,j} \bullet (t_{fluid,j} - t_{W1}) \tag{12}$$

As a result, the convective heat transfer relationship between the inner and outer sides of the condenser tube for a unit length was concluded as Eq. (13):

$$2\pi r_2 \bullet h_{m,outside} \bullet L \bullet (t_{air} - t_{W2}) = \int_0^L 2\pi r_1 \bullet h_{m,inside,j} \bullet (t_{fluid,i} - t_{W1}) \bullet dl \tag{13}$$

where L is the total length of the pipe (m).

The right side of Eq. (13) represented the amount of the heat released during condensation, $\varnothing_{condenser}$, from which the connection between $\varnothing_{condenser}$ and the temperature of the inlet air of outdoor unit was able to be calculated. Eq. (14) was used to calculate $h_{outside}$ in Eq. (13):

$$h_{m,outside} = 0.683 \bullet Re_m^{0.466} \bullet Pr_m^{\frac{1}{3}} \bullet \frac{\lambda_m}{d_2} \tag{14}$$

where $d_2$ is the outer diameter of pipe (m).

The condition parameters of the inlet air of outdoor unit determined each physical parameter in Eq. (14). It was feasible to calculate the numerical variation of the COP at different inlet air temperatures of outdoor unit by obtaining the relationship between the temperature of the inlet air and the cooling capacity at different temperatures.

### 2.5. Prediction of temperature distribution of CFD simulation

CFD simulations in COMSOL were conducted for various structural factors to establish the relationship between designs of cover and the inlet air temperature of the outdoor unit. This process aimed to optimize the structural design of cover. COMSOL Multiphysics software is widely used for CFD simulation, and in the fields of simulation of indoor and outdoor wind environment, it plays a significant role [39–41]. However, due to the time-consuming nature of extensive CFD simulations for structural optimization, this study proposed the use of the GM (1,1) to predict the inlet air temperature under different structural factors. The GA was then applied to refine and optimize the predicted data. The ultimate outcome was the identification of a safe region defined by various structural factors, where the inlet air temperature remains below the safe threshold of 44 °C.

#### 2.5.1. Temperature projection of three dimensions

In this study, the louver cover is characterized by three structural factors: cover angle, cover space, and distance between cover and outdoor unit. Meanwhile, the circular-hole cover consists of two factors: percentage of exposure and distance between cover and outdoor unit. For example, when considering the louver cover, the inlet air temperature under different design conditions creates a 3-D region along three axes, corresponding to the three structural factors. On the other hand, the results for the circular-hole cover form a 2-D region along two axes, corresponding to its two structural factors. Fig. 6 presents the workflow of 3-D projection based on the results of GM (1,1). In Fig. 6(a), the blue sphere represents an instance of the final result for the louver cover, depicting scenarios where the outdoor unit inlet air temperatures remain below 44 °C. Notably, design conditions falling outside this sphere might result in higher temperature faults. For any point $m$ within the sphere, if $D$ denotes the final safe region and $m \in D$, $m$ satisfies the relation expressed in Eq. (15):

$$m \in (AB \cap AC \cap BC) \tag{15}$$

In Eq. (15), AB, AC, and BC represent the three-dimensional projections of three distinct directions. These projections denote the safe regions of two random factors, determined through predictions derived from the GM (1,1) model combined with GA, illustrated in Fig. 6(b). Taking the safe regions on the AB surface as an example (depicted in Fig. 6(c)), these regions were determined collectively by the predicted outcomes of Factor A and Factor B, while Factor C was held at several specific values, as illustrated in Eq. (16):

$$AB = AB_1 \cup AB_2 \cup AB_3 \cdots \cup AB_N \tag{16}$$

where $AB_1 \cdots AB_N$ are the predicted outcomes of Factor A and Factor B, while Factor C was held at several specific values.
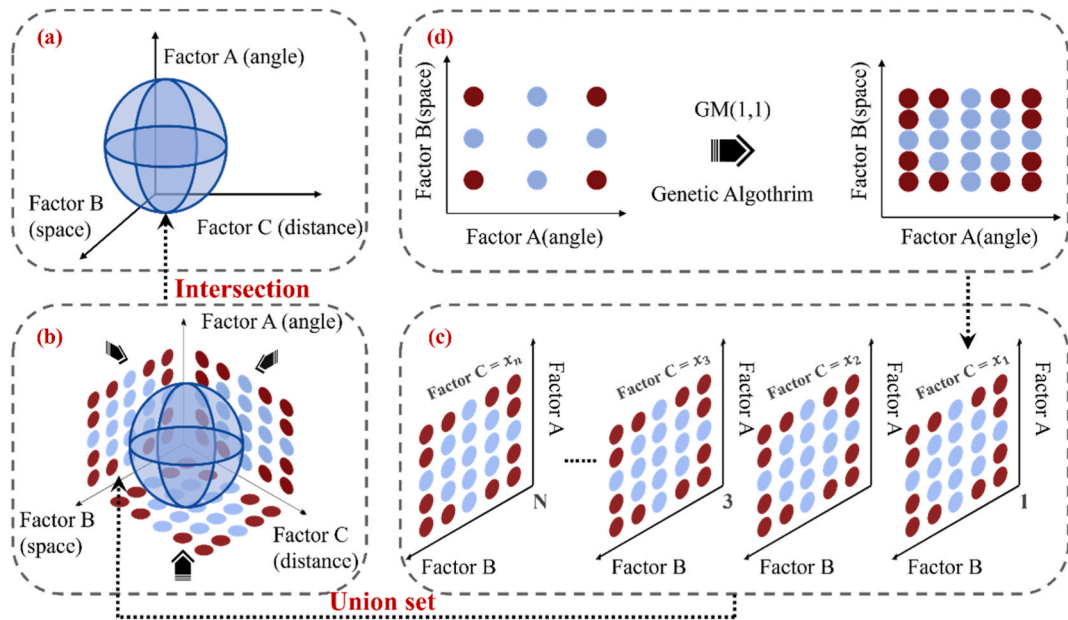


**Fig. 6.** Workflow of 3-D projection and the region formed by the blue points are safe region. **(a).** The sphere is the final prediction result; **(b).** The sphere is the result of intersection of three factors; **(c).** The prediction of Factor A and B is the result of union set of different Factor C; **(d).** GM (1,1) and GA are applied to the prediction of temperature data. (For interpretation of the references to color in this figure legend, the reader is referred to the Web version of this article.)

Similarly, employing this method led to the identification of other safe regions within AC and BC. Ultimately, the only question remaining is how to get the safe region of each different Factor C. Thus, taking AB$_1$ results as examples, as shown in Fig. 6(d), the prediction of GM (1,1) quantitatively expanded the initial CFD simulation data, and GA optimized the prediction result to improve the accuracy of prediction result.

### 2.5.2. Inlet air temperature prediction with the GM (1,1)

The GM (1,1) prediction, GM (1,1), is commonly employed for systems involving uncertain factors. This method entails analyzing correlations among system factors through correlation analysis and processing raw data to uncover patterns in system changes. It is particularly useful for predicting the future development trend of a system [42]. In this study, the primary application of the GM (1,1) involves dataset augmentation, followed by predictions based on outcomes derived from the initial CFD simulation.

As illustrated in Fig. 7, points 1, 2, 3, and 4 represent data obtained from the initial CFD simulation, each corresponding to the maximum inlet air temperature associated with a specific cover structure. Point 5, however, represents the data point to be predicted. This study proposed the following assumptions:

When adjusting the structural factors (Factor A and Factor B) uniformly, the maximum inlet air temperature indicated by the data points varies uniformly without sudden fluctuations.

Consequently, based on these assumptions, the current data points are organized to forecast the next data point, depicted as point 5 in Fig. 7(b). This data ordering follows a changing relationship that initially decreases, then increases, and eventually declines.

In Fig. 7(b), GM (1,1) applied a cumulative summation procedure to mitigate the unpredictability of the data layout, which was represented by Eq. (17):

$$x^{(1)}(t) = \sum_{i=1}^{t} x^{(0)}(i) \tag{17}$$

The solution to the above equation was determined by employing a first order ordinary differential equation (ODE) in Eq. (18) :

$$\frac{dx^{(1)}}{dt} + ax^{(1)} = u \tag{18}$$

Since the data is discrete, the following simplification was obtained in Eq. (19):

$$x^{(0)}(t) = -ax^{(1)}(t) + u \tag{19}$$

In order to further reduce the uncertainty, a weighted sum was computed for each value in the cumulative series. This total was obtained by combining the current term and the prior term, with respective weights M and N in Eq. (20):

$$x^{(1)}(t) = M \bullet x^{(1)}(t) + N \bullet x^{(1)}(t-1) \tag{20}$$

Therefore, the value of $x^{(0)}(t)$ was calculated as Eq. (21):

$$x^{(0)}(t) = -a\big(M \bullet x^{(1)}(t) + N \bullet x^{(1)}(t-1)\big) + u \tag{21}$$

Using the least squares method (OLS), the above equations were solved, which first required the construction of the coefficient matrix in Eqs. (22) and (23):

$$Y = BU \tag{22}$$

$$\begin{bmatrix} x^{(0)}(2) \\ x^{(0)}(3) \\ \vdots \\ x^{(0)}(n) \end{bmatrix} = \begin{bmatrix} -Mx^{(1)}(2) - Nx^{(1)}(1) & 1 \\ -Mx^{(1)}(3) - Nx^{(1)}(2) & 1 \\ \vdots - Mx^{(1)}(n) - Nx^{(1)}(n-1) & \vdots \\ & 1 \end{bmatrix} \begin{bmatrix} a \\ u \end{bmatrix} \tag{23}$$

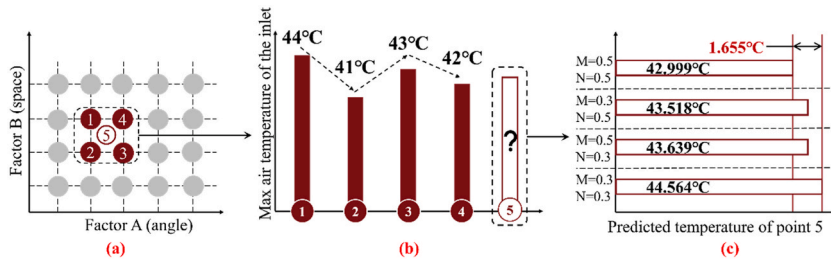Thus, the solution was as Eq. (24):



**Fig. 7.** An example of GM (1,1) for temperature prediction in this study. **(a).** The temperature data of point 5 is predicted by 4 surrounding points; **(b).** The order of dataset for GM (1,1); **(c).** The difference of GM (1,1) results of different M and N in Eq. (21).

$$\widehat{U} = [\widehat{a}, \widehat{b}]^T = \left(B^T B\right)^{-1} B^T Y \tag{24}$$

The solution of Eq. (24) was a definitive conclusion. Nevertheless, it was imperative to evaluate the outcomes of the proposed solution through testing. The evaluation employed two specific tests, namely the relative error test and the stage ratio deviation test, which are Eqs. (25) and (26), respectively. The maximum allowable value for the relative error test is set at 0.2, while the maximum absolute value for the stage ratio deviation test is also limited to 0.2. Predictions are only compliant if they have been used for testing.

$$\varepsilon(t) = \left| \frac{x^{(0)}(t) - \widehat{x}^{(0)}(t)}{x^{(0)}(t)} \right| \tag{25}$$

$$\rho(t) = 1 - \frac{1 - 0.5a}{1 + 0.5a}\lambda(k) = 1 - \frac{1 - 0.5a}{1 + 0.5a} \times \frac{x^{(0)}(t-1)}{x^{(0)}(t)} \tag{26}$$

### 2.5.3. Genetic algorithm

While the GM (1,1) effectively predicts small samples, it still exhibits significant absolute error. Thus, this study directs its focus toward parameters M and N in Eq. (21) to minimize this error, particularly after passing level ratio and relative error tests. Fig. 7(c) demonstrates the substantial impact of altering the values of M and N on the final results, showcasing variations that can lead to an absolute error of 1.655 °C across settings.

Because the optimization problem is a discrete problem, this study employs the GA to determine the optimal values of M and N in Eq. (21) through a calibration process involving the initial prediction outcomes and corresponding simulation data. Table 1 presents this algorithm objective, aiming to reduce the absolute error between predicted and calibrated values to enhance the GM (1,1). The optimized M and N values derived from this process will subsequently inform the following prediction procedures. The crossover rate and mutation rate set in the algorithm are 0.8 and 0.05.

## 3. Results

Upon the methodology introduced by the section before, this section will present the results of thermodynamic calculation and GM (1,1). Results will evaluate quantitatively the impacts of covers on the outdoor units of AC from the aspects of COP and safe operation of AC. For clarity, the results of stationary thermodynamic calculation will be first introduced.

**Table 1**
Workflow of the calibration of GA based on GM (1,1) prediction data.

| Pseudocode of Genetic Algorithm based on the GM (1,1) |
| --- |
| **Input**: calibration value $y_i$; initial data $x^{(0)}_{i(t)}$; Meditations |
| **Define:** predict outcome $x^{(0)}_i$ |
| **Output**: M and N |
| 1: Generate 1-AGO sequence: $x^{(1)}_i(k) = \sum_{t=1}^{k} x^{(0)}_i(t)$ |
| 2: Randomly generate the population of M and N |
| 3: j=1 |
| 4: **while** j <= Meditations |
| 5: **function:** ODE and OLS $[x^{(1)}_i(t), x^{(0)}_i(t), M, N]$ |
| 6:   **return** $[x^{(0)}_i, \max(\varepsilon(t)), \max(\rho(t))]$ |
| 7:   Judge whether the $\max(\varepsilon(t))$ and $\max(\rho(t))$ pass the test |
| 7: **end function** |
| 8:   Calculate $\sum_{i=1} |x^{(0)}_i - y_i|$ |
| 9:   Update the optimal individual |
| 10: **end while** |
| 11: **Return** M and N |

### 3.1. Results of thermodynamic calculation for the impact on COP

Table 2 presents the theoretical calculation parameters. Based on the assumption of thermodynamic calculation, compressor power is constant of 200W and as the most important heat transfer device, condensing tube is single-row and the surface temperature is 60 °C. The inlet air speed was set at 1 m/s. By computing the physical parameters at various inlet temperatures, one can derive the relationship between the AC system's actual cooling capacity and different inlet air temperatures, along with the percentage loss in COP for every 1 °C rise in inlet temperature. As illustrated in Fig. 8, the inlet air temperature increases from 28 °C to 43 °C, resulting in a linear decline in the cooling capacity of AC from 664 W to 263 W. Concurrently, the percentage loss in COP per 1 °C temperature rise shows a consistently upward trend, ranging between a minimum of 4.06% and a maximum of 8.68%. This trend highlights that higher temperatures correspond to more substantial decreases in COP. The fitting of the data yields an R2 value of 0.973, indicating an excellent fit. The fitting function is depicted in Eq. (27):

$$y = 0.33t - 5.96 \tag{27}$$

where $t$ is the inlet air temperature of outdoor unit (°C). $y$ is the percentage of decline of COP (%).

Therefore, the COP variation curve for various inlet air temperatures of the outdoor unit of AC is obtained in Eq. (28):

$$COP = -0.13t + 7.08 \tag{28}$$

As the initial inlet air temperature rises from 28 °C to 43 °C, the COP declines from 3.32 to 1.31. Additionally, subsequent analysis of CFD indicates that inlet air temperature difference of louver cover and circular-hole cover could reach 4.5 °C and 4.1 °C and combined with the relationship of inlet air temperature and COP, the COP reduction percentage could reach 35% and 34% for louver cover and circular-hole cover.

### 3.2. Results of CFD simulation and prediction with GM and GA models

Fig. 9 illustrates the prediction process and results using GM (1,1) and GA for the louver cover. In this instance, the louver angle remains fixed at 65°, while the louver space and distance between cover and outdoor unit serve as independent variables. During the initial COMSOL simulation, the maximum inlet air temperature for each specific cover structure is recorded and displayed by the color of the initial data point. The initial simulation yields 48 data points, which increase to 165 after GM (1,1) prediction. Subsequently, the study employs GA to calibrate the predicted data. The number of data points rises in the second and third GM (1,1), reaching 605 and 2337, respectively. Ultimately, the safe region is determined by excluding data points above 44 °C.

Fig. 10 summarizes the calibration results obtained using GA for the louver cover. This study analyzes the calibration results of the louver cover by considering mean absolute error, maximum absolute error, and mean relative error rates, which involve three structural factors: cover angle, cover space, and the distance between cover and outdoor unit. The findings reveal that adjustments to M and N of Eq. (21) can reduce the maximum absolute error of the three factors by up to 0.38 °C, 1.2 °C, and 1.9 °C, respectively. Additionally, the maximum average absolute error can be decreased by a maximum of 0.08 °C, 0.37 °C, and 0.27 °C, while the average relative error can be reduced to below 1%.

Regarding the circular-hole cover, the maximum absolute error is reduced by 0.53 °C, the mean absolute error is 0.05 °C, and the average relative error is also below 1%. These findings reveal the significant impact of optimizing variables M and N within the GM (1,1) of Eq. (21) for data calibration.

### 3.3. High temperature cause and location

This study utilized a set of temperature probes to pinpoint the location with the highest inlet air temperature under the louver cover, as depicted in Fig. 11. Five location probes were strategically placed on the inlet air surface to gather temperature data, as illustrated in Fig. 11(a). The findings revealed that a significant backflow from the outlet to the inlet led to an increase in the inlet air temperature. Fig. 11(b) indicates that the primary paths for high-temperature backflow are path A and path B, because the high-temperature compressor is located close to the probe 1 and 2, which directly impacts the air temperature of backflow from outlet to inlet.

In most conditions, probe 1 consistently registered the highest inlet air temperature, signifying that the predominant path for high-temperature air backflow is path A. However, as depicted in Fig. 11(c), variations in the structural design factors of the cover notably affect the probability of high-temperature air backflow along path B.

The probability of the highest temperature occurring at probe 2 initially increases and subsequently decreases with Factor C, the distance between the cover and outdoor unit. At a Factor C of 0.25 m, the probability reaches a maximum of 44.4%, while it drops to a minimum of 12.5% at Factor C of 0.40 m. For Factor A, the cover angle below 30° results in a probability below 20%, averaging at 13.9%. Conversely, when the cover angle exceeds 20°, the probability consistently exceeds 25%, averaging at 30.6%. Thus, an increase

**Table 2**
Thermodynamic calculation parameters.

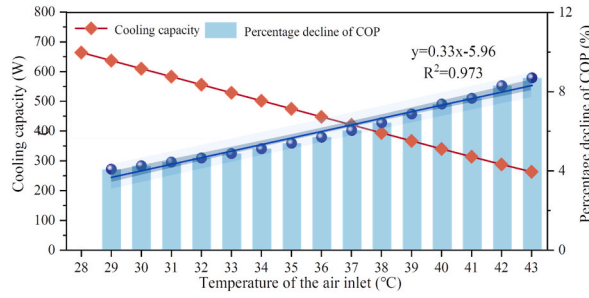| calculating parameter | | | |
|---|---|---|---|
| condensing tube form | single-row | pipe surface temperature (°C) | 60 °C |
| external diameter (mm) | 14 mm | inlet air speed (m/s) | 1 m/s |
| pipe thickness (mm) | 0.7 mm | compressor power (W) | 200 W |

**Fig. 8.** Relationship between the performance of the air condition and the inlet air temperature.
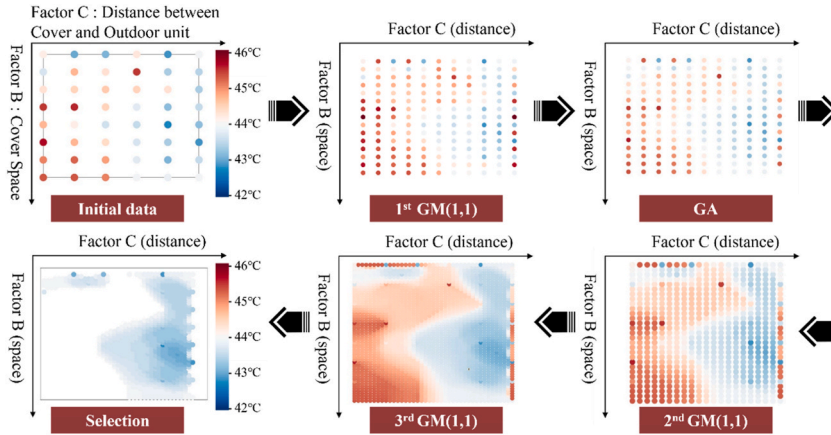


**Fig. 9.** An example of prediction process and results using GM (1,1) and GA models for louver type after CFD simulation.
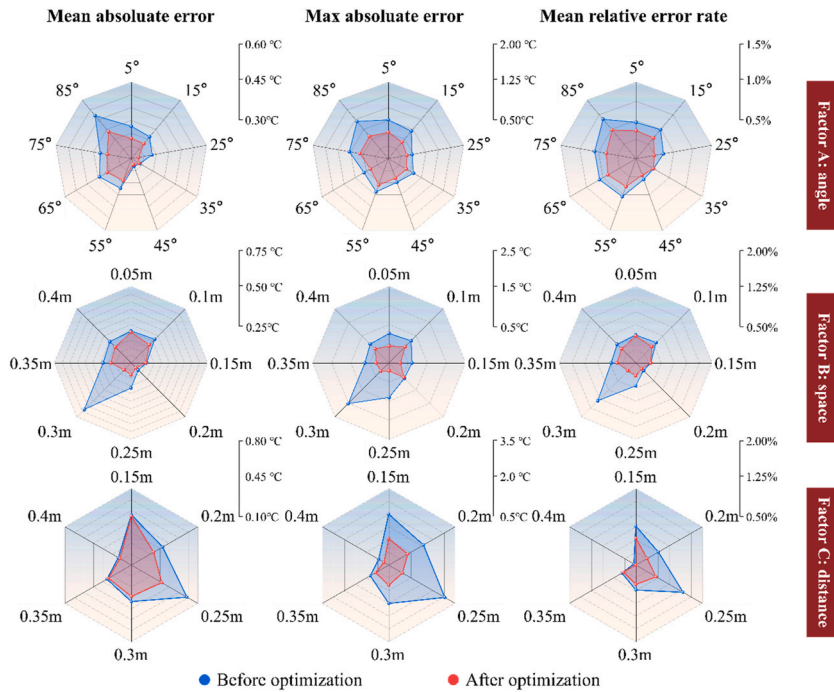


**Fig. 10.** Calibration results of mean absolute error, max absolute error and mean relative error rate louverof three structural design factors for louver cover.
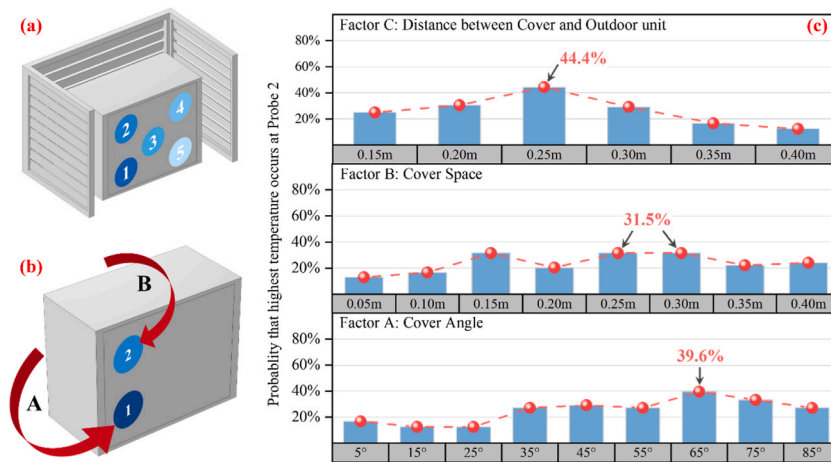
**Fig. 11.** The location with the highest inlet air temperature under the louver cover and its probability of occurrence **(a).** Position of Temperature Probe 1–5; **(b).** High-temperature air return to the air inlet from the outlet; **(c).** The probability changes of the high temperature position occurring in probe 2.

in Factor A indicates a substantial amount of high-temperature air flowing back along path B, ultimately returning to the outdoor unit inlet.

Fig. 12 demonstrates that the rise in inlet air temperature is due to the backflow of high-temperature air from the outlet. Additionally, a comparative analysis indicates that a decrease in the inlet air velocity leads to a rise in the outdoor unit inlet air temperature. Fig. 12 illustrates an increase in the highest inlet air temperature from 43.3 °C to 44.7 °C when the maximum inlet air velocity decreases from 1.5 m/s to 1.0 m/s. This decrease in velocity, owing to the narrow space in front of the inlet caused by the outdoor unit installation against the wall, allows backflow air to absorb significant heat from the outdoor unit high-temperature machine casing. Moreover, as the inlet air velocity decreases, the duration for backflow air to absorb heat from the outlet to the inlet increases, resulting in more heat absorbed by air and higher inlet air temperature for the outdoor unit.

### 3.4. Calibration results of GA

Using GM (1,1) prediction and GA optimization, this study determined the safe operating regions of structural factors for both louverlouver and circular-hole types, ensuring inlet air temperatures remain below 44 °C, which is safe temperature for outdoor unit. In Fig. 13, the safe regions of the louverlouver cover are illustrated, comprising four main regions delineated by a 3-D axis reflecting three structural factors. Specific areas within these four safe regions of the louver cover are detailed in Table 3.

Table 3 demonstrates that when the distance between cover and outdoor unit exceeds 0.29 m, the inlet air temperature consistently stays below 44 °C, irrespective of variations in the other two factors: louver angle and louver space. Additionally, this study assessed the impact of these three structural factors on the probability of inlet temperature surpassing the safe threshold (44 °C) for the louver
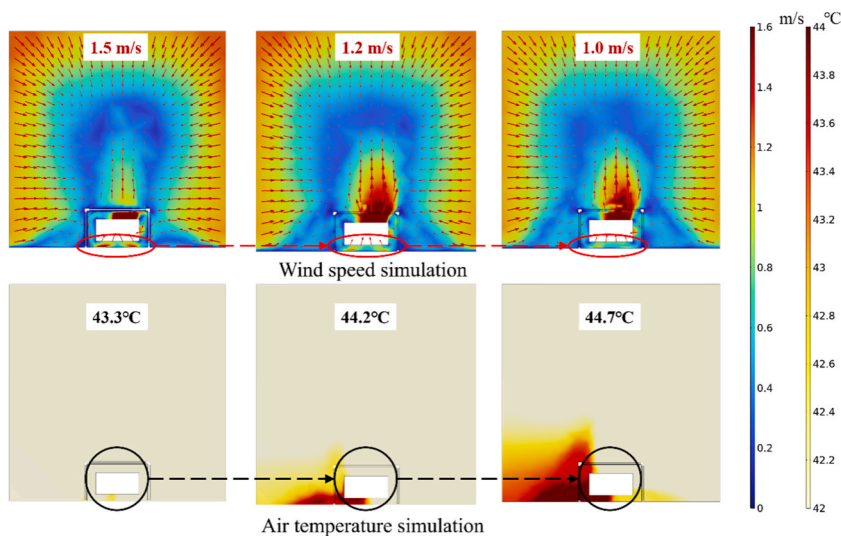


**Fig. 12.** Relationship between high inlet air temperature of outdoor unit and inlet air wind speed.

cover, as depicted in Fig. 14. The findings highlight that Factor C—distance between cover and outdoor unit—exerts the most significant influence. Increasing Factor C from 0.15 m to 0.4 m substantially reduces the probability of high-temperature faults, dropping from 90.2% to 1.4%. Standard deviations for Factor C, A, and B are 38.9, 6.5, and 13.1, respectively, as shown in Table 4. Ultimately, the pivotal factor for the louver cover is Factor C. Once this distance exceeds 0.29 m, the likelihood of high-temperature faults diminishes significantly, regardless of the other two factors' influence.

Conversely, the findings for the circular-hole cover differ significantly from the louver cover. At an ambient temperature of 34 °C, regardless of Factor A (percentage of exposure) and Factor B (distance between cover and outdoor unit), the inlet air temperature remains consistently below 44 °C across all structural design conditions. However, an exception occurs when the distance between the cover and outdoor unit is 0.1 m, and the percentage of exposure is 30%, resulting in the high-temperature fault phenomena. Fig. 15 illustrates that the holes on the left and right sides of the circular-hole cover facilitate easy outflow of high-temperature backflow air from the outlet, dissipating it into the external environment. Thus, for circular-hole cover, it is suggested that distance between cover and outdoor unit keep larger than 0.1 m.

## 4. Discussion

Through on-site investigation in Nanjing city, a popular phenomenon observed is to design and install a cover on outdoor unit of split-air conditioners. With this case, this study would like to answer three questions: i) whether the cover impacts the performance of air conditioners, ii) if yes, what the impact of the cover is, iii) further, how to design the cover to minimize the impact. Therefore, to investigate the impact of cover on the outdoor unit, this study built the thermodynamic model and conducted the airflow simulation with COMSOL software and the GM (1,1) to predict the inlet air temperature of outdoor unit under different structure designs of cover and its impact on COP. The results found the cover installation can impact the COP a lot and the backflow of warm air from the outlet to the inlet and 1 °C rise in inlet air temperature decreases COP by 4.1%–8.7%.

This study can have those implications. First, to ensure normal operation of air conditioners, it is advisable to maintain a minimum distance of 0.29 m between the louver cover and the outdoor unit. For circular-hole covers, a minimum distance of 0.1 m between the cover and the outdoor unit is recommended. In China, installing a cover for outdoor unit of air conditioner is a very common social phenomenon, and its impact is self-evident. These can provide helps to determine the optimal structure designs of covers to minimize the impact on energy use. Second, other popluar installation method of outdoor units is to put on a platform or groove, no matter which way to deal with the outdoor unit, CFD simulation is a common tool to search out optimal solutions, however, it is time-intensive. This study applied GM(1,1) and GAto deal with, which can provide essential insights for those similar issues that use CFD in the optimization. Finally, air conditioners are recognized as one of the main building energy use sectors, while a cover design and installation is proved to possibly increase energy use of air conditioners about 4.1%–8.7% by 1 °C, thus, it is necessary to call for fine design of green building to avoid unnecessary energy loss.

Moreover, this study yields some improvements and future explorations. i) during the investigation of cover types on the outdoor units, it is observed that there are a certain number of outdoor units exposed to the outdoor environment. Thus, the further investigation into how uncovered outdoor units on building facades exacerbate urban heat islands is warranted, also, more parameters could be involved in optimization when installing a cover, e.g., the material types and features (e.g., transparency) of cover, the seasons of weather conditions, and so on; ii) this study proved the significant impact of cover on the COP of AC but how this impact on single building ultimately extend to regional power grid loads and carbon emissions through AC systems is also worth studying, iii) this study revealed the phenomenon of covers surrounding outdoor units, which suggests potential research on how cover might contribute to noise pollution in dense Chinese cities and their influence on indoor thermal comfort, potentially leading to higher energy bills for residents.

## 5. Conclusion

A cover is usually to be installed to conceal the outdoor unit of air conditioners on building facades in most China cities. From on-site investigation in Nanjing city, this study abstracted two popular types of designs of cover(louver and circular-hole) and chose Nanjing, a hot summer city in China, for the case study city. To investigate the impact of the covers on outdoor units, this study established a thermodynamic model to explore the relationship between the COP of air conditioners and the outdoor unit's inlet air temperature, which is directly influenced by the surrounding cover. Additionally, employing the GM (1,1) driven by simulation data using COMSOL software, the study identified safe regions for structural design factors, where maintaining an inlet air temperature below 44 °C is considered a safe threshold. The main findings from this study include the following.

● Theoretical calculations revealed that an increase in the outdoor unit's inlet air temperature from 28 °C to 43 °C resulted in COP reduction of 60.5%. Moreover, the percentage decrease in COP increased from 4.06% to 8.68% for every 1 °C rises in temperature.
● For louver cover, compared with the cover angle and cover space, the distance between cover and outdoor unit makes the biggest difference on the normal performance of outdoor unit. Because of the backflow of high-temperature air from outlet to inlet which is main reason of the fault of outdoor unit, the distance between cover and outdoor unit is more advised to be larger than 0.29 m to maintain the normal performance of outdoor unit.
● Different with the louver cover, the circular-hole cover has lower impact on the performance of outdoor unit because and the suggestion is to maintain the distance between cover and outdoor larger than the 0.1 m. Overall, the circular-hole cover is a more advisable choice for installing covers around the outdoor unit compared to the consideration of a louver cover and its impact on the outdoor unit.
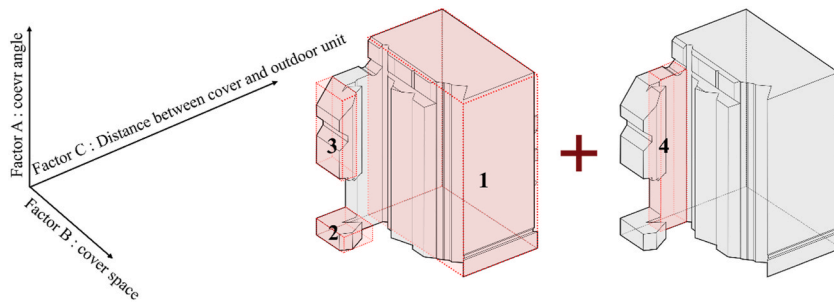
**Fig. 13.** 3D presentation of four safe regions of louver cover with three structural factors as axes.

**Table 3**
Range of three structure parameters of four safe regions of louver cover.

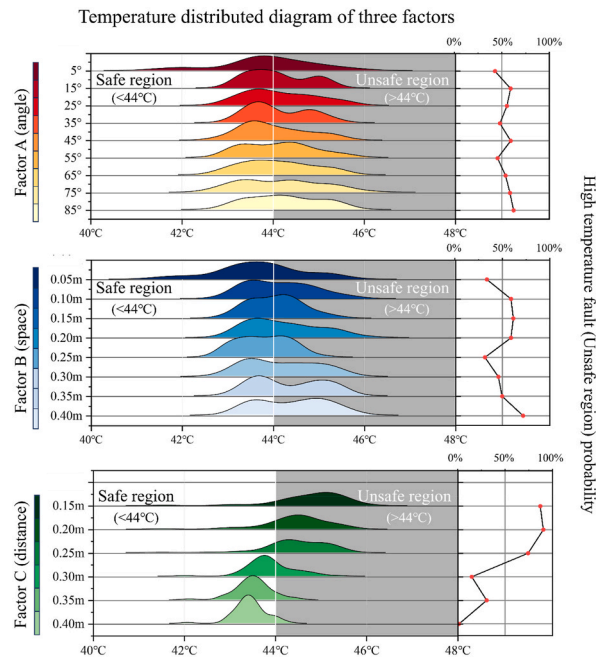| | Minimum Factor A (°) | Maximum Factor A ( ° ) | Minimum Factor B ( m ) | Maximum Factor B (m) | Minimum Factor C (m) | Maximum Factor C (m) |
|---|---|---|---|---|---|---|
| 1 | 5.0° | 85.0° | 0.05 m | 0.40 m | 0.29 m | 0.40 m |
| 2 | 5.0° | 12.5° | 0.05 m | 0.14 m | 0.15 m | 0.21 m |
| 3 | 35.0° | 73.8° | 0.05 m | 0.15 m | 0.15 m | 0.18 m |
| 4 | 5.0° | 72.5° | 0.05 m | 0.09 m | 0.21 m | 0.26 m |



**Fig. 14.** High temperature fault probability of three structural design factors for louver cover.

**Table 4**
Influence index of three structural factors.

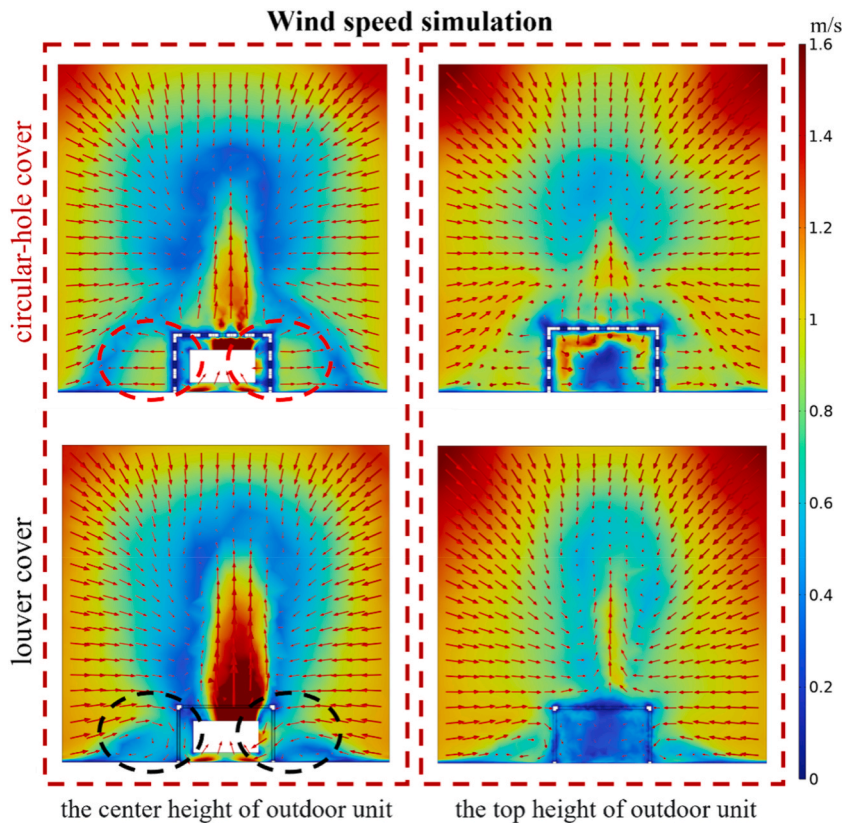| | Factor A | Factor B | Factor C |
|---|---|---|---|
| Average fault rate (%) | 53.8% | 51.5% | 49.6% |
| Maximum fault rate (%) | 62.3% | 71.7% | 90.2% |
| Minimum fault rate (%) | 42.7% | 31.7% | 1.4% |
| Standard deviation | 6.5 | 13.1 | 38.9 |

**Fig. 15.** Reflux condition of louver cover and circular-hole cover.

● This study can serve as a reference for policymakers deciding on the type of cover and whether or not to install it. Furthermore, the results of this study can offer theoretical support for research on carbon emissions from air conditioning systems in urban areas, particularly in instances where the cover is extensively installed around the outdoor unit.

This study's innovations and contributions consist mostly of three parts: i) faced with the need for refined design based on CFD simulation results, this study adopts GM(1,1) combined with GA based on the CFD results to simplify the process of design, which could provide reference for elaborate design involving a large number of simulation processes, ii) thermodynamic model established in this study combined the ambient environment with the COP of AC, which could provide theoretical support for research about the interaction between AC and outdoor, iii) the findings of this study may provide advice and references for installers and policymakers aiming to reduce the negative consequences of covering outdoor unit of AC.

### CRediT authorship contribution statement

**Jiyuan Wu:** Writing – original draft, Methodology, Investigation, Conceptualization. **Lan Wang:** Visualization, Validation. **Tianzhen Hong:** Writing – review & editing, Supervision. **Qinran Hu:** Writing – review & editing. **Wei Wang:** Writing – review & editing, Supervision, Methodology, Investigation, Funding acquisition, Conceptualization.

### Declaration of competing interest

The authors claim no conflicts of interests.

### Data availability

Data will be made available on request.

### Acknowledgement

## References

[1] World meteorological organization, Provisional State of the Global Climate, vol. 2022, 2022. https://digitallibrary.un.org/record/3994344.

[2] National Bureau of statistics of China, China Statistical Yearbook, vol. 2022, 2022. https://www.stats.gov.cn/sj/ndsj/2022/indexch.htm.

[3] J. Shao, Z. Huang, Y. Chen, D. Li, X. Xu, A practical application-oriented model predictive control algorithm for direct expansion (DX) air-conditioning (A/C) systems that balances thermal comfort and energy consumption, Energy 269 (2023), https://doi.org/10.1016/j.energy.2023.126748.

[4] International Energy Agency, Space Cooling, 2023.

[5] Z. Yang, H. Xiao, W. Shi, M. Zhang, B. Wang, Analysis and determination of a seasonal performance evaluation for air source heat pumps, J. Build. Eng. 43 (2021), https://doi.org/10.1016/j.jobe.2021.102574.

[6] B. Bakthavatchalam, K. Habib, R. Saidur, B.B. Saha, Cooling performance analysis of nanofluid assisted novel photovoltaic thermoelectric air conditioner for energy efficient buildings, Appl. Therm. Eng. 213 (2022), https://doi.org/10.1016/j.applthermaleng.2022.118691.

[7] Y. Yadav, A. Kowli, Data-driven simulation for energy and local comfort optimization: case study of a laboratory, J. Build. Eng. 54 (2022), https://doi.org/10.1016/j.jobe.2022.104612.

[8] F. Guo, B. Rasmussen, Predictive maintenance for residential air conditioning systems with smart thermostat data using modified Mann-Kendall tests, Appl. Therm. Eng. 222 (2023), https://doi.org/10.1016/j.applthermaleng.2022.119955.

[9] W.M. Duarte, T.F. Paulino, S.G. Tavares, K.N. Cançado, L. Machado, Comparative study of geothermal and conventional air conditioner: a case of study for office applications, J. Build. Eng. 65 (2023), https://doi.org/10.1016/j.jobe.2022.105786.

[10] K. Zaw, Z.Z.S. Kwik, W.Q. Chang, M.R. Islam, T.K. Poh, A techno-commercial decision support framework for optimal district cooling system design in tropical regions, Appl. Therm. Eng. 220 (2023) 1–10, https://doi.org/10.1016/j.applthermaleng.2022.119668.

[11] N. Sholahudin, Giannetti, Y. Miyaoka, K. Saito, K. Tanaka, H. Ogami, Experimental verification of artificial neural network scalability for performance monitoring of multi-split type air conditioners, J. Build. Eng. 76 (2023) 1–14, https://doi.org/10.1016/j.jobe.2023.107427.

[12] S. Díaz de Garayo, A. Martínez, D. Astrain, Optimal combination of an air-to-air thermoelectric heat pump with a heat recovery system to HVAC a passive house dwelling, Appl. Energy 309 (2022), https://doi.org/10.1016/j.apenergy.2021.118443.

[13] M. Ghodbane, Z. Said, O. Ketfi, B. Boumeddane, A.T. Hoang, M. Sheikholeslami, M.E.H. Assad, M. Hossein Ahmadi, V.N. Nguyen, V.D. Tran, T.H. Truong, Thermal performance assessment of an ejector air-conditioning system with parabolic trough collector using R718 as a refrigerant: a case study in Algerian desert region, Sustain. Energy Technol. Assessments 53 (2022), https://doi.org/10.1016/j.seta.2022.102513.

[14] B. Nagappan, Y. Devarajan, E. Kariappan, Performance analysis of sustainable solar energy operated ejector refrigeration system with the combined effect of Scheffler and parabolic trough collectors to lower greenhouse gases, Environ. Sci. Pollut. Res. 29 (2022) 48411–48423, https://doi.org/10.1007/s11356-022-19058-5.

[15] G. Akkose, C. Meral Akgul, I.G. Dino, Educational building retrofit under climate change and urban heat island effect, J. Build. Eng. 40 (2021), https://doi.org/10.1016/j.jobe.2021.102294.

[16] X. Liu, Y. Ming, Y. Liu, W. Yue, G. Han, Influences of landform and urban form factors on urban heat island: comparative case study between Chengdu and Chongqing, Sci. Total Environ. 820 (2022), https://doi.org/10.1016/j.scitotenv.2022.153395.

[17] F. Marando, M.P. Heris, G. Zulian, A. Udías, L. Mentaschi, N. Chrysoulakis, D. Parastatidis, J. Maes, Urban heat island mitigation by green infrastructure in European Functional Urban Areas, Sustain. Cities Soc. 77 (2022), https://doi.org/10.1016/j.scs.2021.103564.

[18] W. Liang, J. Huang, P. Jones, Q. Wang, J. Hang, A zonal model for assessing street canyon air temperature of high-density cities, Build. Environ. 132 (2018) 160–169, https://doi.org/10.1016/j.buildenv.2018.01.035.

[19] J.S. Lee, J.T. Kim, M.G. Lee, Mitigation of urban heat island effect and greenroofs, Indoor Built Environ. 23 (2014) 62–69, https://doi.org/10.1177/1420326X12474483.

[20] P. Vahmani, X. Luo, A. Jones, T. Hong, Anthropogenic heating of the urban environment: an investigation of feedback dynamics between urban micro-climate and decomposed anthropogenic heating from buildings, Build. Environ. 213 (2022), https://doi.org/10.1016/j.buildenv.2022.108841.

[21] Y.X. Ma, C. Yu, Impact of meteorological factors on high-rise office building energy consumption in Hong Kong: from a spatiotemporal perspective, Energy Build. 228 (2020), https://doi.org/10.1016/j.enbuild.2020.110468.

[22] M. Han, H. Chen, Effect of external air-conditioner units' heat release modes and positions on energy consumption in large public buildings, Build. Environ. 111 (2017) 47–60, https://doi.org/10.1016/j.buildenv.2016.10.014.

[23] C.M. Hsieh, T. Aramaki, K. Hanaki, Managing heat rejected from air conditioning systems to save energy and improve the microclimates of residential buildings, Comput. Environ. Urban Syst. 35 (2011) 358–367, https://doi.org/10.1016/j.compenvurbsys.2011.02.001.

[24] Y.T. Chen, D.S. Lee, Experimental investigation on the improved cooling seasonal performance factor by recycling air flow energy from AC outdoor fans, Case Stud. Therm. Eng. 28 (2021), https://doi.org/10.1016/j.csite.2021.101364.

[25] K.A. Abdullah, R.R.I. Barwari, CFD simulation of thermal plume of VRF air conditioners for cooling season in Semi-Closed spaces for Erbil climate conditions, Int. J. Heat Technol. 40 (2022) 1079–1085, https://doi.org/10.18280/ijht.400426.

[26] M.H. Heydari, G. Heravi, A BIM-based framework for optimization and assessment of buildings' cost and carbon emissions, J. Build. Eng. 79 (2023), https://doi.org/10.1016/j.jobe.2023.107762.

[27] Y.C. Shih, S. Tamilarasan, P.H. Chen, C.C. Tsao, C.H. Lin, Optimal thermohydraulic design of the indoor unit of a split-type air conditioner, Appl. Therm. Eng. 211 (2022), https://doi.org/10.1016/j.applthermaleng.2022.118502.

[28] F. Hou, C. Shen, Q. Cheng, Research on a new optimization method for airflow organization in breeding air conditioning with perforated ceiling ventilation, Energy 254 (2022), https://doi.org/10.1016/j.energy.2022.124279.

[29] X. Liu, M. Wang, H. Liu, W. Chen, S. Qian, Numerical analysis on heat transfer enhancement of wavy fin-tube heat exchangers for air-conditioning applications, Appl. Therm. Eng. 199 (2021), https://doi.org/10.1016/j.applthermaleng.2021.117597.

[30] H.P. Mohammad Hadavi, Investigating effects of urban configuration and density on urban climate and building systems energy consumption, J. Build. Eng. 44 (2021).

[31] Y. Yan, B. Li, Y. Wei, R. Yao, Optimization design of installation platform for outdoor units of residential air conditioners, HV&AC 50 (2020) 19–25 [in Chinese].

[32] X. Xie, X. Liu, C. Blanco, Evaluating and forecasting the niche fitness of regional innovation ecosystems: a comparative evaluation of different optimized grey models, Technol. Forecast. Soc. Change 191 (2023), https://doi.org/10.1016/j.techfore.2023.122473.

[33] L. Liu, Y. Chen, L. Wu, The damping accumulated grey model and its application, Commun. Nonlinear Sci. Numer. Simul. 95 (2021) 1–14, https://doi.org/10.1016/j.cnsns.2020.105665.

[34] Z.X. Wang, Q. Li, Modelling the nonlinear relationship between CO2 emissions and economic growth using a PSO algorithm-based grey Verhulst model, J. Clean. Prod. 207 (2019) 214–224, https://doi.org/10.1016/j.jclepro.2018.10.010.

[35] S. Ding, K.W. Hipel, Y. guo Dang, Forecasting China's electricity consumption using a new grey prediction model, Energy 149 (2018) 314–328, https://doi.org/10.1016/j.energy.2018.01.169.

[36] E. Momeni, R. Nazir, D. Jahed Armaghani, H. Maizir, Prediction of pile bearing capacity using a hybrid genetic algorithm-based ANN, Meas. J. Int. Meas. Confed. 57 (2014) 122–131, https://doi.org/10.1016/j.measurement.2014.08.007.

[37] M. Shariati, S.M. Davoodnabi, A. Toghroli, Z. Kong, A. Shariati, Hybridization of metaheuristic algorithms with adaptive neuro-fuzzy inference system to predict load-slip behavior of angle shear connectors at elevated temperatures, Compos. Struct. 278 (2021), https://doi.org/10.1016/j.compstruct.2021.114524.

[38] National Standards Commission, Room Air Conditioner, 2022. GB/T 7725-2022, https://std.samr.gov.cn/gb/search/gbDetailed?id=EB58F4DA9276B2A2E05397BE0A0A7D33.

[39] J. Shaeri, M. Mahdavinejad, M.H. Pourghasemian, A new design to create natural ventilation in buildings: wind chimney, J. Build. Eng. 59 (2022) 1–23, https://doi.org/10.1016/j.jobe.2022.105041.

[40] P. Li, W. Liu, T. TimZhang, CFD modeling of dynamic airflow and particle transmission in an aircraft lavatory, Build. Simul. (2023) 1375–1390, https://doi.org/10.1007/s12273-023-1031-3.

[41] R. Miao, X. Hu, Y. Yu, Y. Zhang, M. Wood, G. Olson, H. Yang, Evaluation of cooling performance of a novel dual-purpose solar thermal collector through numerical simulations, Appl. Therm. Eng. 204 (2022), https://doi.org/10.1016/j.applthermaleng.2021.117966.

[42] Z.X. Wang, Q. Li, L.L. Pei, A seasonal GM(1,1) model for forecasting the electricity consumption of the primary economic sectors, Energy 154 (2018) 522–534, https://doi.org/10.1016/j.energy.2018.04.155.